

Distributed Brillouin fiber laser sensor

JOSEPH B. MURRAY,^{1,*} ALEX CERJAN,² AND BRANDON REDDING¹

¹U.S. Naval Research Laboratory, 4555 Overlook Ave. SW, Washington 20375, USA

²Center for Integrated Nanotechnologies, Sandia National Laboratories, Albuquerque, New Mexico 87123, USA

*Corresponding author: joseph.murray@nrl.navy.mil

Received 30 June 2021; revised 27 October 2021; accepted 13 December 2021; published 12 January 2022

Brillouin fiber sensors can provide distributed strain and temperature measurements over long distances in standard off-the-shelf fiber by measuring the Brillouin frequency shift as a function of position along a fiber. The primary drawback of these systems is their limited sensitivity, which results from the challenge in identifying the Brillouin frequency shift to within a small fraction of the Brillouin linewidth. In this work, we introduce a technique that overcomes this fundamental limitation by establishing a series of lasing modes that experience Brillouin amplification at discrete spatial locations in the test fiber. The linewidth narrowing and high intensity associated with the lasing transition enable precise measurements of this lasing frequency. As an initial demonstration, we present a sensor that simultaneously excites 40 lasing modes in a 400 m fiber, providing a measurement of the strain at 40 discrete locations with a spatial resolution of 4 m. Each sensor exhibits a minimum detectable strain as low as $4 \text{ ne}/\text{Hz}^{1/2}$ with a dynamic range of $> 5 \text{ me}$ and a bandwidth of $\sim 10 \text{ kHz}$. As the first demonstration that Brillouin lasing can be used for distributed fiber sensing, this work establishes an approach that could enable ultrahigh strain sensitivity using off-the-shelf fiber. © 2022 Optical Society of America under the terms of the OSA Open Access Publishing Agreement

<https://doi.org/10.1364/OPTICA.435716>

1. INTRODUCTION

Brillouin fiber sensors enable fully distributed, absolute strain and temperature measurements in standard off-the-shelf fiber. Many Brillouin sensors also provide a large dynamic range [1–5] and the ability to operate over long distances [6,7] with high spatial resolution [8–13]. These unique features make Brillouin sensors ideally suited for a variety of structural health monitoring applications [14,15]. However, Brillouin sensors struggle to achieve the same sensitivity as competing technologies such as fiber Bragg grating (FBG) sensors or Rayleigh based sensors. This limited sensitivity results from the need to measure the Brillouin resonant frequency to within a small fraction of its linewidth. To fully exploit the many attractive features of Brillouin fiber sensors, a technique capable of achieving higher sensitivity is required.

While an impressive array of Brillouin sensing modalities exists, they all rely on the same basic transduction mechanism: they measure the Brillouin frequency shift, which is a linear function of strain and temperature in the fiber. This is accomplished by measuring either stimulated Brillouin scattering (SBS), as in Brillouin optical time domain analysis (BOTDA), or spontaneous Brillouin scattering (SpBS), as in Brillouin optical time domain reflectometry (BOTDR). SBS based sensors operate by injecting counterpropagating pump and probe beams into the test fiber and typically exhibit lower noise since the SBS process is more efficient. On the other hand, they require access to both ends of the fiber, and the dynamic range is limited by the need to scan or track the relative frequency between the pump and probe beams. In contrast, SpBS based sensors enable single-ended operation by simply injecting

pump light into the fiber and measuring the frequency of the spontaneously backscattered light. This approach enables a large dynamic range, but the weak spontaneous scattering process results in low light levels, and extensive averaging is often required.

Over the past decade, a number of variations on these basic schemes have been introduced to improve the spatial resolution [8–13], dynamic range [1–5], linearity [3,16], signal-to-noise ratio (SNR) [16], and cross talk in these sensors [2,17]. Despite these advances, all of these sensors have to contend with the intrinsically low responsivity of the Brillouin resonance to strain and temperature ($\sim 0.05 \text{ MHz}/\mu\epsilon$ and $\sim 1 \text{ MHz}/\text{K}$) [18]. Although the Brillouin resonance is relatively narrow ($\sim 30 \text{ MHz}$ in standard telecom fiber), detecting small changes in strain or temperature requires the sensor to measure the center of the Brillouin resonance to within a small fraction of its linewidth. For comparison, the resonance of an FBG has a strain response of the order of $100 \text{ MHz}/\mu\epsilon$ [19]. If we consider a standard, commercially available FBG with a linewidth of 1 GHz , detecting $1 \mu\epsilon$ would require the sensor to measure a shift in the resonance by 10% of the full-width at half-maximum (FWHM). In contrast, a Brillouin sensor would need to be sensitive to a shift in the Brillouin resonance as small as 0.17% of the FWHM to detect the same $1 \mu\epsilon$. Since most Brillouin sensors—whether they operate using SBS or SpBS—do not alter the intrinsic linewidth of the Brillouin resonance, high SNR is required to accurately estimate the center of the resonance [16,20,21]. In practice, the situation is even more challenging in many time-domain modalities such as BOTDA, since short pulses effectively broaden the Brillouin linewidth [22]. One notable exception is a technique called gain spectrum engineering, which

combines a series of Stokes and anti-Stokes interactions to narrow the effective Brillouin resonance [23–25]. While this work highlights the potential benefits of altering the resonant linewidth, the narrowest linewidth reported using this approach is ~ 3 MHz [24].

To overcome this inherent limitation, we leverage the linewidth narrowing effect associated with the Brillouin lasing transition to perform precise measurements of the Brillouin resonance. Brillouin fiber lasers can provide exceptionally narrow linewidths due to their ability to suppress the intensity and frequency noise of a pump laser [26–30]. However, Brillouin lasing has rarely been used for sensing, and the only attempts we are aware of were limited to probing a single, extended sensor [31–33]. Here, we introduce a scheme that enables distributed sensing by using a pulsed pump to excite a series of lasing modes in a fiber ring cavity. The lasing modes exhibit linewidths of 4 kHz—four orders of magnitude narrower than the Brillouin gain spectrum. This approach also combines the high intensity and high SNR of SBS based approaches with the large dynamic range of SpBS schemes. These features allow the sensor to achieve a minimum detectable strain of only $4 \text{ ne}/\text{Hz}^{1/2}$ with a dynamic range of $> 5 \text{ me}$ and a bandwidth of ~ 10 kHz.

2. METHOD

The distributed Brillouin laser sensor is designed to excite a series of temporally separated lasing modes that are amplified by SBS in the fiber under test (FUT) at distinct locations. The key components of the sensor are shown in Fig. 1. The system resembles a standard Brillouin fiber ring laser, with a few important distinctions. First, the pump is coupled in and out of the ring cavity using a pair of circulators. This allows for non-resonant coupling, avoiding the need to lock the pump frequency to a cavity resonance [27,28,34]. Second, instead of using a continuous wave (CW) pump, the pump

beam is modulated into a series of pulses similar to a BOTDA or BOTDR measurement. This allows a time-resolved measurement to identify lasing modes that experience Brillouin amplification at different locations in the fiber. When the pump pulse first enters the FUT, it will generate spontaneous Brillouin scattered light traveling in the counterclockwise (CCW) direction through the ring. After circulating through the loop, this spontaneously scattered light will experience amplification by SBS when it interacts with the next pump pulse. Matching the pump pulse period to the round-trip time ensures that this scattered light will experience SBS at the same position after each round trip. If the SBS gain exceeds the round-trip loss in the cavity, the mode will begin to lase. By using this type of ring cavity geometry with pulsed operation, lasing will naturally occur at the frequency with the highest gain, providing a measurement of the Brillouin resonance at the position where a given mode experiences amplification. This is in contrast to CW Brillouin fiber lasers, which lase at the cavity resonance closest to the peak of the gain spectrum [26].

This architecture allows the sensor to excite a series of N lasing modes that experience gain at N positions in the fiber connecting the two circulators. Although the lasing modes circulate in the same ring cavity, they are temporally separated and exhibit distinct lasing frequencies. After each round trip, a fraction of each lasing mode can be removed from the ring cavity, and the lasing frequency can be measured as a function of time to infer the Brillouin frequency as a function of position in the FUT. As in a BOTDA or BOTDR system, the pump pulse duration will dictate the spatial resolution of the system. A diagram of the relative frequencies of three example lasing modes, their respective Brillouin gain spectra, and the pump frequency are shown in Fig. 1(b). This scheme takes advantage of the linewidth narrowing and high intensity associated with the lasing transition to enable a precise measurement of the Brillouin frequency as a function of position in the fiber.

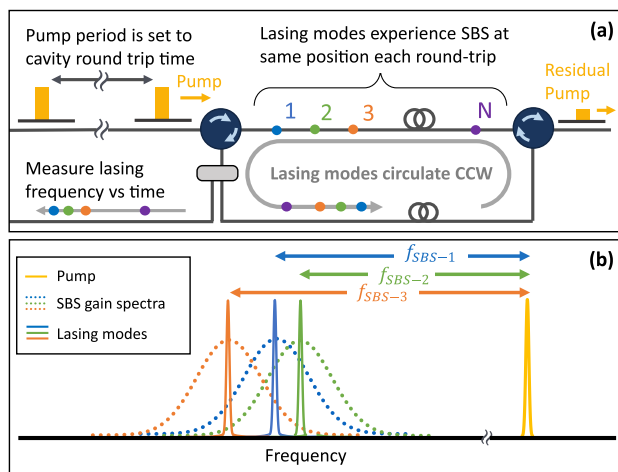


Fig. 1. (a) Distributed Brillouin laser sensor is formed by periodically pumping a fiber ring cavity. The pump pulse repetition period is matched to the round-trip time in the cavity, ensuring that Brillouin scattered light will experience Brillouin amplification at the same position in the fiber after each round trip. A fraction of the lasing light is picked off, and the lasing frequency is measured as a function of time. (b) A pump pulse will create a series of Brillouin gain spectra that are down-shifted by the Brillouin frequency at each position in the fiber. Narrowband lasing will occur at the peak of the gain spectrum at the position where a given mode experiences amplification. The lasing modes are orders of magnitude narrower than the Brillouin gain spectra, enabling precise measurements of the Brillouin frequency.

3. RESULTS

To experimentally realize this scheme, we introduced a few modifications to the basic concept described above. First, we introduce a scheme to compensate for polarization fading and polarization procession, allowing the sensor to use standard single mode fiber as the FUT. Second, we present a technique to compensate for mode competition, enabling the sensor to excite a large number of lasing modes simultaneously.

A schematic of the experimental setup used in this work is shown in Fig. 2. A narrowband CW laser was divided into two paths to generate the pump pulses and a local oscillator (LO). Along the pump path, an electro-optic modulator (EOM₁) was used to generate 40 ns pump pulses with a repetition period of $\sim 5 \mu\text{s}$. The repetition period was fine-tuned to match the round-trip time in the ring cavity. The pump pulses were then directed to a polarization switch consisting of a 2×2 EOM and a polarizing beam splitter (PBS). The 2×2 EOM directed alternating pulses to opposite ports of the PBS, generating sequential pump pulses with orthogonal polarizations. This scheme is often used in BOTDA systems and can efficiently mitigate the effects of polarization fading [35]. A subtle difference here is that due to the circulation of light, averaging of the two polarization states occurs automatically. Finally, the pump pulses were amplified to a peak power of ~ 100 mW before being coupled into the ring cavity through a circulator. A 100 GHz wide wavelength division multiplexing

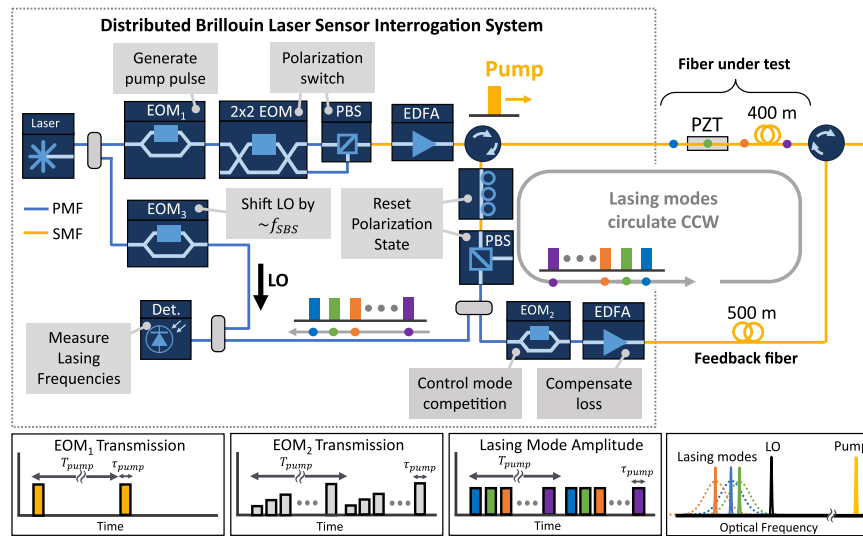


Fig. 2. Experimental setup used to realize the distributed Brillouin laser sensor. The components in the gray dotted box comprise the interrogation system, while the FUT consists of 400 m of fiber with 10 m of fiber mounted on a linear PZT strain stage. A fiber optic circulator and 500 m of additional fiber are used to complete the ring cavity and provide the feedback required for lasing. Note that the blue lines in the schematic indicate polarization maintaining fiber (PMF), while the yellow lines indicate single mode fiber (SMF). 100 GHz WDM filters (not shown) are included after each EDFA to suppress ASE. The lower insets show schematics of the transmission through EOM₁ and EOM₂ the lasing amplitudes in the time domain reaching the photodetector, and the relative frequencies of the pump, LO, and lasing modes.

(WDM) filter was included after the EDFA to suppress amplified spontaneous emission (ASE).

The FUT, or upper portion of the ring cavity, consisted of 400 m of single mode fiber with ~ 10 m of fiber stretched across a linear piezoelectric transducer (PZT) stage positioned 20 m after the first circulator. A second circulator was used to remove the residual pump light from the ring. As in the basic overview shown in Fig. 1, the SBS process will excite lasing modes traveling in the CCW direction. To suppress the effect of polarization procession, the lasing modes were directed through a manual polarization controller and a PBS. The polarization controller was adjusted to minimize loss at the PBS. This ensured that the polarization state of the lasing modes was fixed at the beginning of each round trip. A 90:10 coupler was then used to direct a portion of the lasing modes to a detector where they were combined with the LO.

The remaining 90% of the lasing power was directed to EOM₂ which was used to control mode competition. Mode competition can limit the number of lasing modes excited in the cavity and preclude the system from performing a distributed measurement over the entire FUT. For example, if the lasing modes immediately after the circulator reach threshold first, they can deplete the pump and there may not be enough pump power remaining for later modes to reach their lasing thresholds. To mitigate this effect, we used EOM₂ to adjust the round-trip loss experienced by each mode. This allowed us to compensate for mode competition (e.g., by selectively attenuating the modes at the beginning of the fiber that experiences the highest gain) and enabled multimode lasing. This was achieved by driving EOM₂ with a pulse train with gradually increasing amplitude, as shown schematically in the inset in Fig. 2. The pulse train period was matched to the round-trip time in the cavity, and the individual pulses had the same duration as the pump pulse. Using a pulse train rather than a continuously varying transmission function also allowed us to excite a series of discrete lasing modes (i.e., one mode per pulse). This helped to avoid interference between partially overlapping modes, which could obscure a

measurement of the lasing frequency at a given position. As we will discuss below, pulsing EOM₂ also sets the minimum transform limited bandwidth of the lasing modes, which has implications for the sensor bandwidth.

In the initial demonstrations presented in this work, EOM₂ was driven with a train of 40 pulses separated by 100 ns. The individual pulses were 40 ns in duration (matched to the pump pulse duration) providing a spatial resolution of 4 m, while the 100 ns pulse spacing provided a measurement of the Brillouin frequency in the fiber every 10 m. A simple numerical routine was used to automatically adjust the transmission for each mode until all 40 modes were lasing with comparable amplitude (see Supplement 1 for more detail). This routine required a few seconds to complete and was limited by instrument latency, but could be adapted to periodically adjust the mode-dependent loss to maintain multimode lasing in a deployed system.

Finally, an EDFA was included in the ring cavity to compensate for the insertion loss in EOM₂. This allowed the system to reach the lasing threshold at modest levels of Brillouin gain and to avoid issues associated with pump depletion (e.g., non-local effects [36]). Note that a 100 GHz WDM filter was included after the EDFA to suppress ASE. Since the EDFA gain spectrum is effectively flat across the 100 GHz WDM band, lasing still occurs at the Brillouin frequency. A similar approach has been used in non-resonantly pumped Brillouin fiber lasers to reduce the Brillouin pump power required [26]. After the EDFA, the lasing modes passed through an additional 500 m of fiber before being directed back into the FUT through the second circulator. By making the lower half of the ring cavity longer than the FUT, we ensured that the lasing modes interacted with the pump pulse only once per round trip (i.e., the first lasing pulse must be delayed in the lower half of the cavity for at least the time it takes for the pump pulse to traverse the FUT).

To measure the lasing frequency, the lasing modes were combined with a LO on a 350 MHz photodetector, and the interference signal was digitized at 1 GS/s. The LO was frequency

shifted by driving EOM₃ with a 10.5 GHz tone while it was DC biased for carrier suppression. This created a pair of sidebands at ± 10.5 GHz, close to the ~ 10.6 GHz Brillouin frequency in the FUT. This reduced the intermediate frequency between the lower sideband of the LO and the lasing modes to within the detector bandwidth, while the upper sideband of the LO produced a small DC offset in the detected signal. The relative frequencies of the LO, the pump, and the lasing modes are shown in the lower right inset in Fig. 2.

A typical measurement of the interference pattern produced by the LO mixing with a series of 40 lasing modes is shown in Fig. 3(a). In this case, 40 ns pump pulses were injected into the FUT, providing 4 m spatial resolution, while the pulse train sent to EOM₂ was adjusted to obtain lasing with uniform amplitude across 40 modes separated by 100 ns (corresponding to 10 m spacing in the FUT). The linear strain stage located 20 m into the FUT was used to shift the Brillouin resonance frequency. This location corresponds to the position where the second lasing mode experienced amplification. As a coarse evaluation of the lasing frequency, we calculated the Fourier transform of the interference signal produced by each 40 ns

pulse, as shown in the spectrogram in Fig. 3(b). The Brillouin frequency labeled on the *y* axis was obtained by adding the Fourier frequency to the frequency shift imposed on the LO. This spectrogram showed that the Brillouin frequency at the position where the second lasing mode experienced gain (i.e., on the PZT stage) was shifted by ~ 30 MHz with respect to the Brillouin frequency in the rest of the fiber. Note that this spectrogram, showing the Brillouin frequency at each position in the fiber, was obtained from a single measurement of the lasing modes acquired in just 4 μ s. The high intensity of the lasing modes allows the system to quickly characterize the Brillouin frequency throughout the FUT without requiring the extensive averaging typical of BOTDR and many BOTDA systems.

To more accurately estimate the lasing frequency, we used quadrature demodulation (I/Q demodulation) to extract the amplitude and phase of each mode from the interference pattern shown in Fig. 3(a). The amplitude and phase for the first and second lasing modes are shown in Figs. 3(c) and 3(d). The slope of the phase provides a measurement of the intermediate frequency

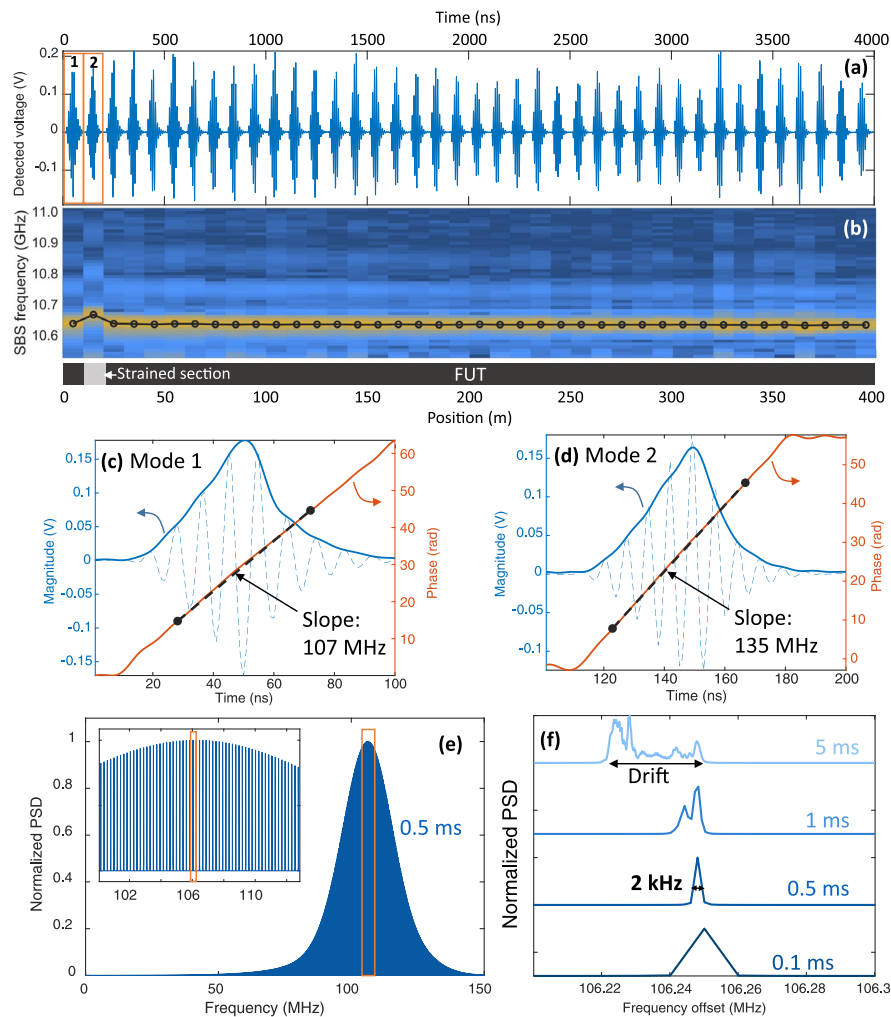


Fig. 3. (a) Measured interference pattern produced by the LO mixing with a series of 40 lasing modes. (b) Spectrogram showing the Fourier transform of each 40 ns pulse in (a). The change in Brillouin frequency at the PZT stage 20 m into the fiber is clearly visible. (c), (d) Interference pattern (blue dashed lines) and demodulated amplitude (blue solid lines) along with the demodulated phase for the first two lasing modes. The slope of the phase was used to estimate the Brillouin frequency. (e) PSD of the interference pattern produced by the first lasing mode and the LO recorded over 1 ms. The width of an individual comb tooth is shown in (f) for varying acquisition time. The minimum linewidth of 4 kHz indicates that the lasing linewidth is four orders of magnitude narrower than the Brillouin gain spectrum.

between the LO and the lasing mode and can be used to calculate the Brillouin frequency as $f_{\text{SBS}} = f_{\text{EOM}_3} + [d\phi/dt]/(2\pi)$, where f_{EOM_3} is the 10.53 GHz frequency shift applied to the LO. Here, we calculated the slope of the phase for each mode using a linear fit over the 40 ns with the highest magnitude. This approach showed that the Brillouin frequency at the first sensor position was 10.637 GHz, while the strain introduced by the PZT shifted the Brillouin frequency at the second sensor position by 28 MHz to 10.665 GHz.

This initial analysis showed that this approach can enable single-shot measurements of the Brillouin frequency with a large dynamic range (limited only by the detector and digitizer bandwidth). However, our primary motivation for using the lasing phenomena was to leverage the linewidth narrowing effect to more accurately measure the Brillouin frequency. Due to the short temporal duration of the lasing pulses, their transform limited bandwidth remains relatively broad at 25 MHz for a 40 ns pulse. However, such a single-shot analysis neglects the pulse-to-pulse coherence, which makes the lasing modes resemble an optical frequency comb. Thus, to analyze the linewidth of the lasing modes, we adopted a technique commonly used to characterize frequency combs [37,38]. We first recorded a 5 ms dataset consisting of 1000 measurements of the lasing pulse train interfering with the LO. We then applied a 100 ns Hanning window to select the first lasing mode in each pulse train. Finally, we calculated the power spectral density (PSD) of the windowed interference signal over varying lengths of time. A typical PSD obtained in this manner is shown in Fig. 3(e), revealing a series of lines spaced by ~ 200 kHz (i.e., the pulse repetition period), characteristic of an optical frequency comb. In Fig. 3(f), we show the linewidth of an individual comb tooth calculated using varying integration times. The minimum linewidth, obtained using a 0.5 ms integration time, was 2 kHz,

which is four orders of magnitude narrower than the Brillouin linewidth. The linewidth broadened slightly in longer datasets, likely due to environmental drift in the relative phase between the LO and the lasing mode. Nonetheless, this dramatic linewidth reduction illustrates the potential for this approach to identify the Brillouin resonance with unprecedented accuracy.

We then conducted a series of experiments to quantitatively evaluate the sensor performance. First, we collected a series of static measurements while gradually increasing the strain on the PZT stage to evaluate the linearity and dynamic range of the sensor. The Brillouin frequency at each sensor position was extracted by calculating the slope of the demodulated phase, as described above. As shown in Fig. 4(a), the Brillouin frequency at the PZT position increased linearly with strain while the Brillouin frequency at the remaining positions was unaffected. This measurement also confirmed that the sensor exhibited the expected response of ~ 0.05 MHz/ $\mu\epsilon$ [18] and exhibited a dynamic range of at least 5 m ϵ , approaching the damage threshold of the fiber. The cross talk experienced by the remaining modes was below -47 dB, despite the fact that every lasing mode passes through the strained section of fiber. This confirmed the basic operating premise of the sensor: that each mode's lasing frequency is dictated by the Brillouin frequency at the position where a mode experiences gain and is independent of the Brillouin resonance in the rest of the fiber or the length of the ring cavity.

We then evaluated the ability of the sensor to measure dynamic strain. While the sensor obtains a measurement of the Brillouin frequency after each round trip, two additional factors can influence the actual sensor bandwidth. The first factor to consider is how quickly the lasing mode changes frequency when the Brillouin frequency changes. Consider the case in which a lasing mode is already established at the center of the Brillouin gain spectrum

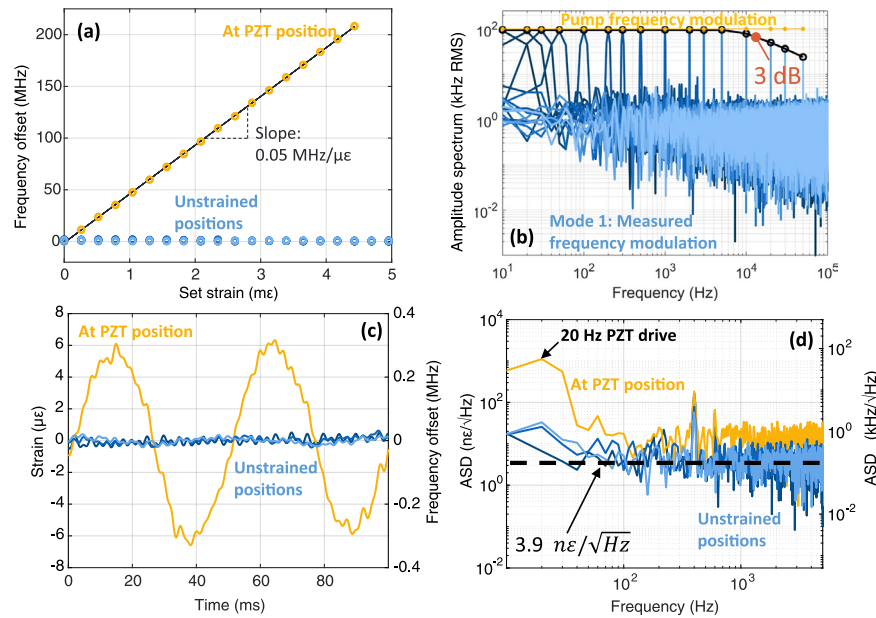


Fig. 4. (a) In the static regime, the sensor accurately tracked the change in Brillouin frequency as strain was applied to the PZT stage. The Brillouin frequencies measured at the remaining sensor positions were unaffected. (b) The sensor response time was measured by modulating the pump frequency with a deviation of 100 kHz at varying frequencies from 10 Hz to 50 kHz. The measured modulation in the Brillouin frequency accurately tracks the pump modulation up to a 3 dB bandwidth of ~ 10 kHz. (c) Time-varying strain recovered from the first four lasing modes while a dynamic, 20 Hz sinusoidal strain was applied to the PZT. The lasing mode under strain clearly tracks the PZT modulation, while the remaining modes were unaffected. Note that a 600 Hz low pass filter was applied for clarity. (d) Amplitude spectral density for the same 100 ms long dataset shown in (c). The 20 Hz modulation is observed at the PZT position with an average cross talk below -29 dB. This ASD also provided a measurement of the minimum detectable strain.

when the gain spectrum suddenly shifts due to strain in the fiber. Since the lasing mode is no longer centered at the peak of the gain spectrum, gain pulling will eventually shift the lasing frequency back to the center (see Supplement 1 for further discussion). However, the efficiency of the gain pulling effect depends on the instantaneous bandwidth of the lasing mode, since gain pulling relies on selectively amplifying the spectral components of the mode that overlap with the peak of the gain spectrum. As a result, shorter pulses will respond faster to a change in the Brillouin frequency due to their broader transform limited bandwidth. In our experiments, the 40 ns pulse duration set by EOM₁ and EOM₂ ensures that the lasing modes have a transform limited bandwidth of ~ 25 MHz. To evaluate the effective bandwidth of the sensor, we modulated the pump frequency by inserting an acousto-optic modulator (AOM) before EOM₁. Modulating the pump frequency shifts the Brillouin gain spectrum relative to the lasing mode and allowed us to evaluate the sensor response over a wide range of frequencies (including frequencies beyond the PZT bandwidth). The pump frequency was modulated with a deviation of 100 kHz at varying frequencies from 10 Hz to 50 kHz. The amplitude spectrum of the measured lasing frequency is presented in Fig. 4(b). The response of the first lasing mode is shown in the figure, but each mode showed a similar response. We found that the lasing mode efficiently tracked the change in the pump frequency up to ~ 5 kHz. However, above ~ 5 kHz, the lasing frequency struggled to keep up with the change in the pump frequency, and the response began to fall off, resulting in a 3 dB reduction in responsivity at 10 kHz. While this bandwidth is already sufficient for most applications, we expect that a higher bandwidth would be possible by using shorter pulses (see Supplement 1 for further discussion). Last, we can use this measurement to estimate the sensor slew rate, or the maximum change in Brillouin frequency per round trip that the sensor can track. Based on the measured 5 kHz bandwidth observed for a 100 kHz modulation, this test indicates a maximum slew rate of ~ 3 GHz/s, equivalent to ~ 60 m ϵ /s.

The second factor influencing the ability of the sensor to measure dynamic strains is the sensitivity to strain-induced Doppler shifts in the cavity itself, which can introduce cross talk. If part of the FUT is exposed to a time-varying strain, any light passing through this section of fiber will experience a Doppler shift. This effect can introduce significant levels of cross talk in standard Brillouin sensors (e.g., BOTDA) exposed to dynamic strain [16,17]. In this system, the lasing modes are potentially even more sensitive to strain-induced Doppler shifts since the lasing modes can pass through a strained region of fiber many times, gradually accumulating a larger and larger frequency shift. Fortunately, the gain pulling effect will partially counteract this phenomenon by shifting the lasing frequency back toward the center of the Brillouin gain spectrum after each round trip.

While we were able to perform dynamic strain measurements at low frequencies with modest levels of cross talk, the effect was more significant than in a BOTDA system. To compensate for this effect, we investigated a technique to monitor any strain-induced Doppler shifts in the FUT and remove their impact from the measured Brillouin frequencies. We used a separate low-power reference laser to measure the Doppler shift in the FUT and introduced a reference PZT to provide a calibration signal. We then computationally removed the Doppler shift experienced by each lasing mode using the frequency shift measured by the reference laser (see Supplement 1 for details). To test the efficacy of this

approach, we introduced a 20 Hz modulation to the linear strain stage as a test signal. The time-varying strain (derived from the time-varying lasing frequency) measured by the first four lasing modes are shown in Fig. 4(c). The suppression is quite effective, and the strain modulation is observed only by the second lasing mode, as expected. This also indicated that effects such as pump depletion [3,36,39] did not introduce significant levels of cross talk even though the pump pulse passed through the strained section of fiber before exciting subsequent lasing modes. The corresponding amplitude spectral densities (ASDs) obtained for these four lasing modes are shown in Fig. 4(d), indicating cross talk of -29 dB. The ASDs shown in Fig. 4(d) also reveal that the sensor exhibited a minimum detectable strain of only 3.9 n ϵ /Hz^{1/2}. This corresponds to a minimum detectable frequency shift of ~ 100 Hz/Hz^{1/2}.

The Brillouin laser sensor presented here exhibits substantially lower strain noise than state-of-the-art Brillouin sensors at this length scale. For example, Yang *et al.* presented a BOTDA scheme that achieved a strain noise of ~ 100 n ϵ /Hz^{1/2} in 2 km of fiber with 2.5 m resolution [3]. Similarly, Peled *et al.* reported ~ 220 n ϵ /Hz^{1/2} in 100 m of fiber with 1 m resolution [40]. We recently described a slope-assisted BOTDA system that was optimized for low-noise operation and achieved a strain noise of 19.8 n ϵ /Hz^{1/2} in 1 km of fiber [16]. Note that these BOTDA based approaches provide continuously distributed measurements, in contrast to the series of discrete measurements obtained using the sensor presented in this work. Of course, these BOTDA systems also have a limited dynamic range compared with the Brillouin laser sensor. Many BOTDR systems can provide a dynamic range similar to the Brillouin laser sensor presented here, but with much lower sensitivity: typically > 10 $\mu\epsilon$ /Hz^{1/2} [41].

While other fiber sensing modalities such as Rayleigh scattering based ϕ -OTDR systems can achieve lower noise, they do not provide the absolute strain measurements or large dynamic range achieved here [42]. Compared with an FBG based system, the Brillouin laser sensor enables the use of off-the-shelf fiber, and the sensors can be repositioned on demand. While the system presented here was designed to probe 40 locations along a 400 m FUT, there is significant potential to increase the sensor count and length of the FUT. The spatial resolution could also be improved by reducing the pump pulse duration, although the phonon lifetime would likely limit the resolution to ~ 1 m [43]. There are also several paths to reduce the system complexity and number of required components. For example, a semiconductor optical amplifier could be used to replace EOM₂ and the EDFA in the loop both by providing amplification and compensating for mode competition. In addition, EOM₃ (used to shift the LO frequency), could be replaced with a Brillouin laser following the technique described in [44], or neglected entirely by simply using a high bandwidth detector to measure the Brillouin frequency shift directly.

4. CONCLUSION

In summary, this paper introduced a technique to perform distributed strain sensing by exciting a series of Brillouin lasing modes in a fiber ring cavity. We described the basic sensor concept along with techniques to address polarization fading and mode competition. As a proof-of-principle demonstration, we presented a sensor that simultaneously excited 40 lasing modes, providing a measurement of the Brillouin frequency at 40 locations along a 400 m test fiber.

The lasing modes exhibited a narrow linewidth of 4 kHz, compared to the 30 MHz linewidth of the Brillouin gain spectrum. The narrow linewidth and high intensity of the lasing modes enabled the sensor to achieve a minimum detectable strain of only $4 \text{ n}\epsilon/\text{Hz}^{1/2}$ combined with a dynamic range of $>5 \text{ m}\epsilon$. We also showed that this approach is capable of performing dynamic strain measurements and described a technique to address cross talk due to strain-induced Doppler shifts. While considerable optimization is still required to realize the full potential of this new approach, the sensor presented here already provides record sensitivity for a Brillouin sensor at this length scale.

Funding. Laboratory Directed Research and Development, Sandia National Laboratories; U.S. Naval Research Laboratory.

Acknowledgment. This work was supported by the US Naval Research Laboratory. A.C. recognizes the support of the Center for Integrated Nanotechnologies, an Office of Science User Facility operated for the U.S. Department of Energy (DOE) Office of Science. Sandia National Laboratories is a multimission laboratory managed and operated by National Technology & Engineering Solutions of Sandia, LLC, a wholly owned subsidiary of Honeywell International, Inc., for the U.S. DOE's National Nuclear Security Administration under contract DE-NA-0003525. The views expressed in the article do not necessarily represent the views of the U.S. DOE or the United States Government.

Disclosures. The authors declare no competing interests.

Data availability. All data are available in the main text or [Supplement 1](#) and are available from the corresponding author upon reasonable request.

Supplemental document. See [Supplement 1](#) for supporting content.

REFERENCES

- H. Zheng, D. Feng, J. Zhang, T. Zhu, Y. Bai, D. Qu, X. Huang, and F. Qiu, "Distributed vibration measurement based on a coherent multi-slope-assisted BOTDA with a large dynamic range," *Opt. Lett.* **44**, 1245–1248 (2019).
- J. Urricelqui, A. Zornoza, M. Sagues, and A. Loayssa, "Dynamic BOTDA measurements based on Brillouin phase-shift and RF demodulation," *Opt. Express* **20**, 26942–26949 (2012).
- G. Yang, X. Fan, and Z. He, "Strain dynamic range enlargement of slope-assisted BOTDA by using Brillouin phase-gain ratio," *J. Lightwave Technol.* **35**, 4451–4458 (2017).
- D. Zhou, Y. Dong, B. Wang, T. Jiang, D. Ba, P. Xu, H. Zhang, Z. Lu, and H. Li, "Slope-assisted BOTDA based on vector SBS and frequency-agile technique for wide-strain-range dynamic measurements," *Opt. Express* **25**, 1889–1902 (2017).
- Z. Yang, M. A. Soto, D. M. Chow, P. Ray, and L. Thevenaz, "Brillouin distributed optical fiber sensor based on a closed-loop configuration," *J. Lightwave Technol.* **36**, 1239–1248 (2018).
- M. A. Soto, G. Bolognini, and F. Di Pasquale, "Optimization of long-range BOTDA sensors with high resolution using first-order bi-directional Raman amplification," *Opt. Express* **19**, 4444–4457 (2011).
- M. A. Soto, G. Bolognini, and F. Di Pasquale, "Long-range simplex-coded BOTDA sensor over 120km distance employing optical preamplification," *Opt. Lett.* **36**, 232–234 (2011).
- K. Y. Song, Z. He, and K. Hotate, "Distributed strain measurement with millimeter-order spatial resolution based on Brillouin optical correlation domain analysis and beat lock-in detection scheme," *Opt. Lett.* **31**, 2526–2528 (2006).
- A. W. Brown, B. G. Colpitts, and K. Brown, "Dark-pulse Brillouin optical time-domain sensor with 20-mm spatial resolution," *J. Lightwave Technol.* **25**, 381–386 (2007).
- A. Bergman, T. Langer, and M. Tur, "Coding-enhanced ultrafast and distributed Brillouin dynamic gratings sensing using coherent detection," *J. Lightwave Technol.* **34**, 5593–5600 (2016).
- Y. Dong, H. Zhang, L. Chen, and X. Bao, "2 cm spatial-resolution and 2 km range Brillouin optical fiber sensor using a transient differential pulse pair," *Appl. Opt.* **51**, 1229–1235 (2012).
- W. Li, X. Bao, Y. Li, and L. Chen, "Differential pulse-width pair BOTDA for high spatial resolution sensing," *Opt. Express* **16**, 21616–21625 (2008).
- A. Dominguez-Lopez, M. A. Soto, S. Martin-Lopez, L. Thevenaz, and M. Gonzalez-Herraez, "Resolving 1 million sensing points in an optimized differential time-domain Brillouin sensor," *Opt. Lett.* **42**, 1903–1906 (2017).
- P. Ferdinand, "The evolution of optical fiber sensors technologies during the 35 last years and their applications in structure health monitoring," in *EWSHM - 7th European Workshop on Structural Health Monitoring*, L. Cam, M. Vincent, and S. Laurent, eds. (2014).
- A. Barrias, J. R. Casas, and S. Villalba, "A review of distributed optical fiber sensors for civil engineering applications," *Sensors* **16**, 748 (2016).
- J. B. Murray and B. Redding, "Combining Stokes and anti-Stokes interactions to achieve ultra-low noise dynamic Brillouin strain sensing," *APL Photon.* **5**, 116104 (2020).
- J. B. Murray and B. Redding, "Suppressing non-local effects due to Doppler frequency shifts in dynamic Brillouin fiber sensors," *Opt. Express* **28**, 10760–10771 (2020).
- A. Motil, A. Bergman, and M. Tur, "[Invited] state of the art of Brillouin fiber-optic distributed sensing," *Opt. Laser Technol.* **78**, 81–103 (2016).
- A. Othonos, "Fiber Bragg gratings," *Rev. Sci. Instrum.* **68**, 4309–4341 (1997).
- A. Lopez-Gil, M. A. Soto, X. Angulo-Vinuesa, A. Dominguez-Lopez, S. Martin-Lopez, L. Thévenaz, and M. Gonzalez-Herraez, "Evaluation of the accuracy of BOTDA systems based on the phase spectral response," *Opt. Express* **24**, 17200–17214 (2016).
- M. A. Soto and L. Thévenaz, "Modeling and evaluating the performance of Brillouin distributed optical fiber sensors," *Opt. Express* **21**, 31347–31366 (2013).
- A. Fellay, L. Thévenaz, M. Facchini, M. Niklès, and P. Robert, "Distributed sensing using stimulated Brillouin scattering: towards ultimate resolution," in *12th International Conference on Optical Fiber Sensors* (Optical Society of America, 1997), paper OWD3.
- C. Feng, X. Lu, S. Preussler, and T. Schneider, "Gain spectrum engineering in distributed Brillouin fiber sensors," *J. Lightwave Technol.* **37**, 5231–5237 (2019).
- S. Preußler, A. Wiatrek, K. Jamshidi, and T. Schneider, "Brillouin scattering gain bandwidth reduction down to 3.4MHz," *Opt. Express* **19**, 8565–8570 (2011).
- C. Feng and T. Schneider, "Benefits of spectral property engineering in distributed Brillouin fiber sensing," *Sensors* **21**, 1881 (2021).
- M. Chen, C. Wang, J. Wang, H. Luo, and Z. Meng, "53-dB phase noise suppression and Hz-range linewidth emission in compact Brillouin/erbium fiber laser," *Opt. Express* **25**, 19216–19225 (2017).
- M. Chen, Z. Meng, X. Tu, and H. Zhou, "Low-noise, single-frequency, single-polarization Brillouin/erbium fiber laser," *Opt. Lett.* **38**, 2041–2043 (2013).
- M. Chen, Z. Meng, X. Tu, and Y. Zhang, "Fast-tuning, low-noise, compact Brillouin/erbium fiber laser," *Opt. Lett.* **39**, 689–692 (2014).
- S. P. Smith, F. Zarinetchi, and S. Ezekiel, "Narrow-linewidth stimulated Brillouin fiber laser and applications," *Opt. Lett.* **16**, 393–395 (1991).
- A. Debut, S. Randoux, and J. Zemmouri, "Linewidth narrowing in Brillouin lasers: theoretical analysis," *Phys. Rev. A* **62**, 023803 (2000).
- Y. Liu and M. Zhang, "Multiwavelength Brillouin erbium fiber laser sensor with high resolution," in *Conference on Lasers and Electro-Optics Pacific Rim (CLEO-PR)* (2017), pp. 1–3.
- H. Xie, J. Shao, Z. Sun, and J. Sun, "Simultaneous measurement of strain and temperature based on radio-frequency demodulation," *IEEE Photon. Technol. Lett.* **29**, 623–626 (2017).
- H. Xie, J. Sun, and D. Feng, "Simultaneous measurement of strain and temperature based on hybrid EDF/Brillouin laser," *Opt. Express* **24**, 11475–11482 (2016).
- G. J. Cowle and D. Y. Stepanov, "Hybrid Brillouin/erbium fiber laser," *Opt. Lett.* **21**, 1250–1252 (1996).
- K. Hotate, K. Abe, and K. Y. Song, "Suppression of signal fluctuation in Brillouin optical correlation domain analysis system using polarization diversity scheme," *IEEE Photon. Technol. Lett.* **18**, 2653–2655 (2006).
- L. Thévenaz, S. F. Mafang, and J. Lin, "Effect of pulse depletion in a Brillouin optical time-domain analysis system," *Opt. Express* **21**, 14017–14035 (2013).
- N. Coluccelli, M. Cassinerio, A. Gambetta, P. Laporta, and G. Galzerano, "Frequency-noise measurements of optical frequency combs by multiple fringe-side discriminator," *Sci. Rep.* **5**, 16338 (2015).
- K. Kim, J. W. Nicholson, M. Yan, J. C. Knight, N. R. Newbury, and S. A. Diddams, "Characterization of frequency noise on a broadband infrared

- frequency comb using optical heterodyne techniques," *Opt. Express* **15**, 17715–17723 (2007).
39. H. Iribas, J. Urricelqui, J. J. Mompó, J. Mariñelarena, and A. Loayssa, "Non-local effects in Brillouin optical time-domain analysis sensors," *Appl. Sci.* **7**, 761 (2017).
40. Y. Peled, A. Motil, and M. Tur, "Fast Brillouin optical time domain analysis for dynamic sensing," *Opt. Express* **20**, 8584–8591 (2012).
41. Q. Bai, Q. Wang, D. Wang, Y. Wang, Y. Gao, H. Zhang, M. Zhang, and B. Jin, "Recent advances in Brillouin optical time domain reflectometry," *Sensors* **19**, 1862 (2019).
42. A. Masoudi and T. P. Newson, "Contributed review: distributed optical fibre dynamic strain sensing," *Rev. Sci. Instrum.* **87**, 011501 (2016).
43. H. Naruse and M. Tateda, "Trade-off between the spatial and the frequency resolutions in measuring the power spectrum of the Brillouin backscattered light in an optical fiber," *Appl. Opt.* **38**, 6516–6521 (1999).
44. D. Marini, M. Iuliano, F. Bastianini, and G. Bolognini, "BOTDA sensing employing a modified Brillouin fiber laser probe source," *J. Lightwave Technol.* **36**, 1131–1137 (2018).